Comparative Study of Sinc Collocation Method versus Hybrid Sinc-Finite Difference Methods for Solving Burgers' Equations

Moayad Odeh, Martin Mohlenkamp, Muhammad Usman, Todd Young

***Abstract*—We present a Sinc Collocation Method (SCM) with Double Exponential (DE) Transformations, and compare it with the Hybrid Sinc-Finite Difference Method by Wang, Li, and Meng on Burgers' equations. Sinc collocation promises exponential order convergence for smooth problems. The DE transformation allows this promise to be realized by mapping a finite interval domain to the real line. It increases the density of collocations points near the ends of the interval, which allows it to achieve high accuracy and order both at the collocation points and between them. In contrast, we show that the hybrid method has much larger errors between collocation points due to Runge's phenomenon. For the time discretization, we use Crank-Nicolson for the linear part and Heun's method for the nonlinear part and observe second-order accuracy. Comparative analysis with the Hybrid Sinc method confirms SCM's superior performance across various initial conditions and discretization settings.**

***Index Terms*—Burgers' Equation, Coupled Burgers' Equation, Exponential Transformations, Sinc Collocation, Hybrid Sinc-Finite Difference, Runge's Phenomenon.**

I. INTRODUCTION

A. Burgers' Equations

BURGERS'equation is a specific form of advection-diffusion equation [1] that describes various physical phenomena, including fluid dynamics, gas dynamics, traffic flow [2], [3], [4], and nonlinear acoustics [5]. It was first formulated by Harry Bateman in 1915 [6], [2] and later extensively analyzed by Johannes Martinus Burgers in 1948 [7]. It has come to be considered as a prototype for nonlinear parabolic equations. Coupled Burgers' equations play a significant role in physics, particularly in understanding fluid dynamics and related phenomena [8], [9].

The general form of the Burgers' equation in one dimension is given by [10]:

$$u_t(x,t) = Du_{xx}(x,t) - uu_x(x,t), \tag{1}$$

for $0 < x < L$, and $0 < t < T$, where $D > 0$ is the diffusion coefficient. The equation models the interaction between nonlinear convection and diffusion. We consider an initial condition:

$$u(x,0) = f(x), \tag{2}$$

with homogeneous Dirichlet boundary conditions

$$u(0,t) = 0, \quad u(L,t) = 0. \tag{3}$$

The coupled equations have the form [10]:

$$\begin{aligned} u_t &= D_1 u_{xx} - \eta u u_x - \alpha(uv)_x, \\ v_t &= D_2 v_{xx} - \xi v v_x - \beta(uv)_x, \end{aligned} \tag{4}$$

where D_1, D_2, η, ξ, α, and β are constants that depend on the system properties. The initial conditions are

$$u(x,0) = f(x), \quad v(x,0) = g(x), \tag{5}$$

and the homogeneous Dirichlet boundary conditions are

$$u(0,t) = u(L,t) = v(0,t) = v(L,t) = 0. \tag{6}$$

B. Previous Work on Numerical Solutions of Burgers' Equations

The numerical solution of Burgers' equation has been widely studied and has been important in various applied fields. Numerous numerical techniques have been developed, encompassing a wide range of analytical approaches and computational strategies. For example, there are cubic B-splines collocation methods [11], finite difference methods [12], the fourth-order singly diagonally implicit Runge-Kutta method [13], the Chebyshev Wavelet Method [14], finite element methods [15], and, the Milne method [16].

For the discretization in time, the Crank-Nicolson (C-N) method [17] is usually adequate for the linear part of the equation, since it is second-order, unconditionally stable, and only requires solving a linear system. One must then decide whether to treat the non-linear part of the equation explicitly (simple but only first order), implicitly (requiring solving a nonlinear system), or by some other method.

For the discretization in space, one could use a Finite Difference Method (FDM) [18]. Mitchell and Griffiths [19] provided a comprehensive review of FDMs applied to parabolic equations. While the FDM is effective in many applications, on a straightforward equally-spaced discretization it is limited to second order. As an alternative, spectral methods, including the Sinc collocation method, have gained popularity due to their exponential convergence properties, especially for smooth problems [20], [21].

The Sinc-Galerkin method, introduced by Stenger [21], has been extensively studied for solving partial differential equations and was later extended by Lund and Bowers [22] to handle more complex boundary value problems. In recent years, the combination of Sinc collocation methods with

Manuscript received November 20, 2024; revised April 16, 2025.

M. Odeh is a Ph.D. candidate in Mathematics at Ohio University, Athens, OH 45701, USA. (corresponding author to provide e-mail: mo174820@ohio.edu).

M. Mohlenkamp is a Professor of Mathematics at Ohio University, Athens, OH 45701, USA (e-mail: mohlenka@ohio.edu).

M. Usman is a Professor of Mathematics at the University of Dayton, Dayton, OH 45469, USA (e-mail: musman1@udayton.edu).

T. Young is a Professor of Mathematics at Ohio University, Athens, OH 45701, USA (e-mail: youngt@ohio.edu).

conformal mapping has further improved their accuracy and efficiency. Double exponential (DE) transformations, introduced by Takahashi and Mori [23], have been effective in handling boundary layers and singularly perturbed equations. Single exponential (SE) transformations offer a simpler approach while still achieving rapid convergence, as demonstrated by M. Mori and M. Sugihara [24].

Recently, Wang et al. [10] used a hybrid method combining the Sinc collocation method and central finite differences to solve single and coupled Burgers' equations. The Sinc collocation method was applied at the k-th time step to approximate the first-order spatial derivative, while central finite difference formulas were used at the $(k+1)$-st time step for both first-order and second-order spatial derivatives. This hybrid approach was intended to blend the accuracy of Sinc collocation with the computational simplicity of finite differences. They conducted extensive numerical tests to assess the accuracy, efficiency and stability of their method on several examples. They showed that their method is accurate and stable. We will compare our work with [10] due to its clarity and replicable results.

C. Summary of Our Results

In this paper we propose a new strategy. We use a C-N scheme for the time discretization of linear terms combined with Heun's method (also known as Modified Euler) discretization for the nonlinear terms. In space, we use the Sinc collocation combined with DE conformal mappings for the spatial discretization, including all spatial derivatives.

We demonstrate numerically that this strategy is significantly more accurate than the Sinc-Hybrid method in Wang [10] and greatly outperforms the C-N FDM approximation when applied to Burgers' equations. Specifically:

- The combination of C-N for the linear terms and Heun for the nonlinear term achieves second order accuracy in time with small constant, without resorting to a nonlinear solve.
- The new method achieves high order convergence (up to order 8) in the spatial variable.
- The Sinc-Hybrid method suffers from Runge's phenomenon with large errors between collocation points, while the new method does not.

D. Organization of the Paper

In Section II, we present the general parabolic PDE system in vector form. Section III details Sinc Interpolation, covering the derivation of Sinc functions, matrix construction for derivatives, the application of Single and Double Exponential transformations.

Section IV outlines the time discretization using a combination of the Crank-Nicolson method and Heun's method, resulting in a time-discretized form. Section V focuses on the space discretization using the Sinc Collocation Method (SCM), and includes the truncated cardinal series approximation and matrix formulations. Section VI combines the spatial and time discretizations to yield a fully discretized system and then discusses its linear stability.

In Section VII, we present the numerical solutions, including error calculations. This section applies the numerical scheme and a few other methods to Burgers' equations and compares the results with [10].

Finally, Section VIII presents the conclusion, summarizing the results and providing comparisons with [10].

II. General Parabolic System of Equations

A general system of μ coupled parabolic partial differential equations (PDEs) on the one-dimensional spatial domain $x \in [a,b]$ can be written in vector form as

$$\mathbf{u}_t(x,t) = \nabla^2 \mathbf{u}(x,t)\mathbf{D} + \mathbf{Q}(x,t,\mathbf{u}(x,t),\mathbf{u}_x(x,t)), \quad (7)$$

where $\mathbf{D}$ is a diagonal diffusion coefficient matrix, and $\mathbf{Q}(x,t,\mathbf{u}(x,t),\mathbf{u}_x(x,t))$ represents the nonlinear convection and interaction terms.

We take $\mathbf{u}(x,t)$ and $\mathbf{Q}(x,t,\mathbf{u}(x,t),\mathbf{u}_x(x,t))$ to be row vectors with entries $u_i(x,t)$ and $Q_i(x,t,\mathbf{u}(x,t),\mathbf{u}_x(x,t))$ for $i = 1,\ldots,\mu$.

The system is subject to the initial conditions:

$$u_i(x,0) = f_i(x), \quad i = 1,\ldots,\mu. \quad (8)$$

In this paper, we will consider the homogeneous boundary conditions $\mathbf{u}(a,t) = \mathbf{0}$ and $\mathbf{u}(b,t) = \mathbf{0}$ in order to compare our results with [10].

A. Burgers' Equation

For $\mu = 1$ and setting $\mathbf{Q}(x,t,\mathbf{u},\mathbf{u}_x) = -uu_x$, we obtain the Burgers' equation, as presented in (1).

For $\mu = 2$, the coupled Burgers' equations (4) are obtained by setting $\mathbf{u} = (u,v)$ and $\mathbf{Q}(x,t,\mathbf{u},\mathbf{u}_x) = \begin{pmatrix} -\eta_1 uu_x - \xi_1(uv)_x \\ -\eta_2 vv_x - \xi_2(uv)_x \end{pmatrix}^T$ in (7). The initial and boundary conditions are specified in (2) and (3), and D_1, D_2, η_1, η_2, ξ_1, and ξ_2 represent system-dependent constants.

III. Sinc Interpolation

A. The Sinc Function

We begin by introducing the Sinc function, which forms the foundation of our approximation procedure.

Definition 3.1 (p. 5, [22]): The Sinc function, defined for all $x \in \mathbb{R}$, is given by

$$\operatorname{sinc}(x) = \begin{cases} \frac{\sin(\pi x)}{\pi x} & \text{if} \quad x \neq 0, \\ 1 & \text{if} \quad x = 0. \end{cases} \quad (9)$$

For each integer j and mesh size $h > 0$, the Sinc basis functions on $\mathbb{R}$ are defined as:

$$S(j,h)(x) \equiv \operatorname{sinc}\left(\frac{x-jh}{h}\right) = \begin{cases} \frac{\sin\left(\frac{\pi(x-jh)}{h}\right)}{\frac{\pi(x-jh)}{h}} & \text{if} \quad x \neq jh, \\ 1 & \text{if} \quad x = jh. \end{cases} \quad (10)$$

Three representative translated Sinc functions (10) are shown in Figure 1.

The Whittaker cardinal expansion [25] of a function f on $\mathbb{R}$ is defined as follows.

Definition 3.2 (p. 22, [22]): Let f be a function defined on $\mathbb{R}$ and let $h > 0$. Define the series

$$C(f,h)(x) = \sum_{j=-\infty}^{\infty} f(jh)S(j,h)(x), \quad (11)$$

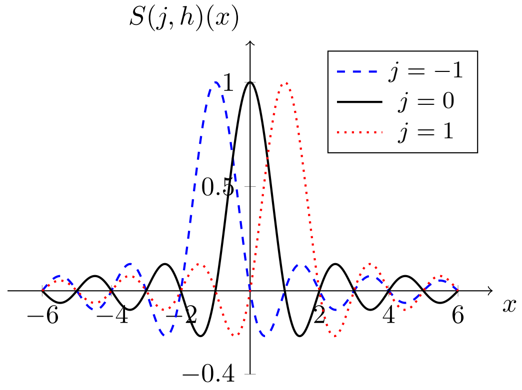

Fig. 1: An illustration of three translated Sinc basis functions at $j=-1,0,1$ with mesh size $h=1$.

where $S(j,h)(x)$ is given by (10). Whenever the series in (11) converges, it is called the cardinal function of f.
For our numerical method, we will use the truncated cardinal series which is defined as

$$C_{M_x,N_x}(f,h)(x) = \sum_{j=-M_x}^{N_x} f(jh)S(j,h)(x), \tag{12}$$

for appropriate values of N_x and M_x.

The Sinc series converges exponentially fast for certain analytic functions. If f is analytic and uniformly bounded on the strip

$$D_d = \{z \in \mathbb{C} : |\Im z| < d\}, \tag{13}$$

then the following error bound holds [26]:

$$\sup_{x\in\mathbb{R}} |f(x) - C(f,h)(x)| = \mathcal{O}(e^{-\pi d/h}), \quad h \to 0.$$

Due to its exponential convergence, the Sinc series is potentially a powerful tool for solving PDEs.

B. Conformal Map Definitions

As noted above, the Sinc method theoretically achieves exponential convergence on an infinite domain. For problems defined on finite intervals, we employ a conformal mapping to preserve this exponential error decay. Specifically, following the approach in [26], we use a conformal transformation that maps the finite interval to the real line, where the Sinc basis functions are applied. To approximate a function F over an finite interval Γ, we select a transformation ϕ that provides a one-to-one mapping of Γ onto $\mathbb{R}$. The problem of approximating F on Γ is transformed to the task of approximating $f = F \circ \phi^{-1}$ on $\mathbb{R}$. It is ideal to choose transformations ϕ that can be clearly expressed, and for which the inverse ϕ^{-1} can be easily calculated. Here are two conformal mappings that we will consider.

The Single Exponential (SE) transformation (p. 63, 91, [22]) maps the finite interval $\Gamma = (a,b)$ to $(-\infty,\infty)$ and is defined as:

$$w = \phi_{SE}(z) = \log\left(\frac{z-a}{b-z}\right). \tag{14}$$

The function ϕ_{SE} provides a conformal transformation of:

$$\mathcal{D} = \{z \in \mathbb{C} : |\arg\left(\frac{z-a}{b-z}\right)| < d\} \tag{15}$$

onto the strip D_d, as in (13). The inverse transformation is given by:

$$z = \phi_{SE}^{-1}(\omega) = \frac{a + b\cdot e^{\omega}}{1+e^{\omega}}.$$

The equally spaced nodes $kh \in (-\infty,\infty)$ correspond to the nodes:

$$x_k = \phi_{SE}^{-1}(kh) = \frac{a + b\cdot e^{kh}}{1+e^{kh}} \in (a,b) = \Gamma. \tag{16}$$

The Double Exponential (DE) Transformation [26], [27], [28] is used to improve accuracy by increasing the density of points near the boundaries. This transformation maps the finite interval (a,b) to $(-\infty,\infty)$ by

$$w = \phi_{DE}(z) = \operatorname{arcsinh}\left(\frac{2}{\pi}\operatorname{arctanh}\left(\frac{2z}{b-a} + \frac{a+b}{a-b}\right)\right). \tag{17}$$

The function ϕ_{DE} provides a conformal transformation of a (hard to describe) region $\mathcal{D}$ onto the strip D_d in (13). The equally spaced nodes $kh \in (-\infty,\infty)$ correspond to the nodes

$$\begin{aligned} x_k = \phi_{DE}^{-1}(kh) = {} & \frac{(b-a)}{2}\cdot\tanh\left(\frac{\pi}{2}\cdot\sinh(kh)\right) \\ & + \frac{a+b}{2} \in (a,b) = \Gamma. \end{aligned} \tag{18}$$

This mapping clusters points near boundaries, enhancing numerical accuracy and allowing Sinc collocation to be applied efficiently to bounded domains.

Equally spaced nodes $kh \in (-\infty,\infty)$ become non-uniformly spaced in the original interval,

$$x_k = \phi^{-1}(kh) \in (a,b),$$

with points clustering near the boundaries. This non-uniform distribution improves the accuracy of the Sinc approximation, especially for problems where boundary behavior is critical.

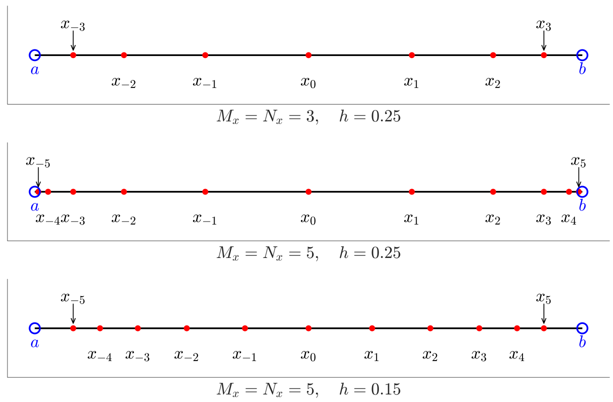

Fig. 2: Distribution of collocation points with different $M_x = N_x$ values.

In Figure 2, we illustrate the distribution of collocation points with different $M_x = N_x$ values. Increasing $M_x = N_x$ (fixed h) adds more points at the boundaries, while leaving the interior points unchanged. Decreasing h (fixed $M_x = N_x$) refines the spacing, densifying points across the entire domain. By simultaneously adjusting $M_x = N_x$ and h, we can systematically increase the approximation accuracy of the method.

The basis functions for the Sinc method applied to the interval (a, b) are

$$S(j,h) \circ \phi(z) = \mathrm{sinc}\left(\frac{\phi(z) - jh}{h}\right). \tag{19}$$

The truncated cardinal Sinc series as in (12) becomes the composite truncated cardinal Sinc series

$$C_{M_x,N_x}(f,h,\phi)(x) = \sum_{j=-M_x}^{N_x} f(jh)\mathrm{sinc}\left(\frac{\phi(x) - jh}{h}\right). \tag{20}$$

To represent the function F on the interval (a, b), recall $F = f \circ \phi$, so (20) becomes

$$\begin{aligned}\sum_{j=-M_x}^{N_x} & F(\phi^{-1}(jh))\mathrm{sinc}\left(\frac{\phi(x) - jh}{h}\right) \\ &= \sum_{j=-M_x}^{N_x} F(x_j)\mathrm{sinc}\left(\frac{\phi(x) - jh}{h}\right).\end{aligned}$$

Additionally, it is important to note the boundary behavior of the Sinc function. Specifically,

$$\begin{aligned}\lim_{x\to a^+} & \left(\mathrm{sinc}\left(\frac{\phi(x) - jh}{h}\right)\right) \\ &= \lim_{w\to-\infty}\left(\mathrm{sinc}\left(\frac{w - jh}{h}\right)\right) = 0,\end{aligned} \tag{21}$$

and similarly as $x \to b^-$. This ensures that the Sinc approximation handles zero boundary conditions naturally.

C. Sinc Derivative Approximations

The derivatives of the truncated composite Sinc function in (20) are computed at the Sinc nodes $x_k = \phi^{-1}(kh)$ using the following lemma.

Lemma 1 ([22], p. 106): Let ϕ be a conformal one-to-one map of the simply connected domain $\mathcal{D}$ onto D_d. Then

$$\delta_{jk}^{(0)} \equiv [S(j,h) \circ \phi(x)]\Big|_{x=x_k} = \begin{cases} 1, & j = k, \\ 0, & j \neq k, \end{cases} \tag{22}$$

$$\delta_{jk}^{(1)} \equiv h\frac{d}{d\phi}\left[S(j,h) \circ \phi(x)\right]\Big|_{x=x_k} = \begin{cases} 0, & j = k, \\ \frac{(-1)^{k-j}}{k-j}, & j \neq k, \end{cases} \tag{23}$$

and

$$\delta_{jk}^{(2)} \equiv h^2\frac{d^2}{d\phi^2}\left[S(j,h) \circ \phi(x)\right]\Big|_{x=x_k} = \begin{cases} -\frac{\pi^2}{3}, & j = k, \\ \frac{-2(-1)^{k-j}}{(k-j)^2}, & j \neq k. \end{cases} \tag{24}$$

In the relations (22)–(24), h is the step size and $x_k = \phi^{-1}(kh)$ is the Sinc grid in the original domain.

Note that $\delta_{jk}^{(0)} = \delta_{kj}^{(0)}$, $\delta_{jk}^{(1)} = -\delta_{kj}^{(1)}$, and $\delta_{jk}^{(2)} = \delta_{kj}^{(2)}$. We define the $m \times m$ matrices,

$$I_{m\times m}^{(\ell)} \equiv \left[\delta_{jk}^{(\ell)}\right], \quad \ell = 0, 1, 2, \tag{25}$$

where $\delta_{jk}^{(\ell)}$ denotes the (j, k)-th element of the matrix $I^{(\ell)}$ and $m = M_x + N_x + 1$. Note that the matrix $I^{(0)}$ is the identity matrix, $I^{(1)}$ is skew-symmetric, and $I^{(2)}$ is symmetric.

IV. Time Discretization

To discretize the time derivative in (7), we divide the time interval $[0, T]$ into N equal sub-intervals with step size $\Delta t = T/N$. We approximate the time derivative $\mathbf{u}_t$ as

$$\mathbf{u}_t \approx \frac{\mathbf{u}^{n+1} - \mathbf{u}^n}{\Delta t},$$

where $\mathbf{u}^n$ and $\mathbf{u}^{n+1}$ represent the solution at time steps t^n and t^{n+1}, respectively.

We approximate the linear spatial term $\nabla^2\mathbf{u}$ using a weighted average between the current and next time steps:

$$\nabla^2\mathbf{u} \approx \theta\mathbf{u}_{xx}^{n+1} + (1-\theta)\mathbf{u}_{xx}^n, \tag{26}$$

where $0 \leq \theta \leq 1$ controls the weighting. Setting $\theta = \frac{1}{2}$ corresponds to the standard C-N method, providing second-order accuracy in time for the linear part of the equation [22].

To avoid solving nonlinear equations at each time step, we approximate the nonlinear term $\mathbf{Q}$ at the current time step:

$$\mathbf{Q}(x, t, \mathbf{u}, \mathbf{u}_x) \approx \mathbf{Q}(x, t^n, \mathbf{u}^n, \mathbf{u}_x^n). \tag{27}$$

Incorporating these discretizations, we have

$$\begin{aligned}\frac{\mathbf{u}^{n+1} - \mathbf{u}^n}{\Delta t} &= \theta\mathbf{u}_{xx}^{n+1}\mathbf{D} + (1-\theta)\mathbf{u}_{xx}^n\mathbf{D} \\ &\quad + \mathbf{Q}(x, t^n, \mathbf{u}^n, \mathbf{u}_x^n) + \mathbf{R}^{n+1},\end{aligned} \tag{28}$$

where $\mathbf{R}^{n+1}$ is the truncation error. By omitting $\mathbf{R}^{n+1}$, the time discretization equation becomes

$$\begin{aligned}\mathbf{U}^{n+1} - \Delta t\theta\mathbf{D}\mathbf{U}_{xx}^{n+1} &= \mathbf{U}^n + \Delta t(1-\theta)\mathbf{D}\mathbf{U}_{xx}^n \\ &\quad + \Delta t\mathbf{Q}(x, t^n, \mathbf{U}^n, \mathbf{U}_x^n),\end{aligned} \tag{29}$$

where $\mathbf{U}^{n+1} = \mathbf{U}(x, t_{n+1})$ is the solution of (29) at the $(n + 1)$-st time level, given $\mathbf{U}^n$.

If we solve for $\mathbf{U}^{n+1}$ using (29), it results in a first-order method since the nonlinear part is treated explicitly. We may improve upon this by introducing a predictor-corrector approach based on Heun's method (also known as the modified Euler method).

The first step (Predictor) of our method is to solve for $\mathbf{V}^{n+1}$ in (29),

$$\begin{aligned}\mathbf{V}^{n+1} - \Delta t\theta\mathbf{D}\mathbf{V}_{xx}^{n+1} &= \mathbf{U}^n + \Delta t(1-\theta)\mathbf{D}\mathbf{U}_{xx}^n \\ &\quad + \Delta t\,\mathbf{Q}(x, t^n, \mathbf{U}^n, \mathbf{U}_x^n).\end{aligned} \tag{30}$$

Then, the second step (Corrector) is to solve for $\mathbf{U}^{n+1}$ using an improved approximation of $\mathbf{Q}(x, t, \mathbf{U}, \mathbf{U}_x)$

$$\begin{aligned}\mathbf{U}^{n+1} - \Delta t\theta\mathbf{D}\mathbf{U}_{xx}^{n+1} &= \mathbf{U}^n + \Delta t(1-\theta)\mathbf{D}\mathbf{U}_{xx}^n \\ &+ \frac{\Delta t}{2}\left(\mathbf{Q}(x, t^n, \mathbf{U}^n, \mathbf{U}_x^n) + \mathbf{Q}(x, t^{n+1}, \mathbf{V}^{n+1}, \mathbf{V}_x^{n+1})\right).\end{aligned} \tag{31}$$

This two-step semi-implicit method [29] combines the Crank-Nicolson scheme for the linear diffusion term with Heun's method for the nonlinear reaction term. It is expected to be second-order in time, which is confirmed by our numerical solutions in Section VII.

V. Space Discretization

We will apply the Sinc Collocation Method (SCM) to (29) and (31) in the spatial variable. To simplify the exposition, we present the method as applied to (29), We may derive a similar full discretization for (31) (Huen's method applied to the nonlinearity).

A. Truncated Cardinal Series Approximation

We approximate $\mathbf{u}(x, t^{n+1})$ using the truncated cardinal series:

$$\mathbf{U}^{n+1}(x) = \sum_{j=-M_x}^{N_x} \mathbf{c}_j{}^{n+1} S(j,h) \circ \phi(x), \tag{32}$$

where,

$$\mathbf{U}^{n+1}(x) = \left(U_1^{n+1}(x), \quad \cdots, \quad U_\mu^{n+1}(x)\right),$$
$$\mathbf{c}_j{}^{n+1} = \left(c_{j,1}^{n+1}, \quad c_{j,2}^{n+1}, \quad \cdots, \quad c_{j,\mu}^{n+1}\right).$$

Let C^{n+1} be the matrix collecting the row vectors $\mathbf{c}_j{}^{n+1}$, with entries $C^{n+1}(j,i) = c_{j,i}^{n+1}$.

1) Boundary Properties and Differentiation: Due to the properties of the Sinc function (21), the approximation $\mathbf{U}^{n+1}(x)$ satisfies:

$$\lim_{x\to a^+} \mathbf{U}^{n+1}(x) = \lim_{x \to b^-} \mathbf{U}^{n+1}(x) = \mathbf{0}. \tag{33}$$

Differentiating $\mathbf{U}^{n+1}(x)$ yields

$$\mathbf{U}_x^{n+1}(x) = \sum_{j=-M_x}^{N_x} \mathbf{c}_j{}^{n+1} \left[\frac{dS(j,h)\circ\phi(x)}{d\phi(x)} \frac{d\phi(x)}{dx}\right], \tag{34}$$

$$\mathbf{U}_{xx}^{n+1}(x) = \sum_{j=-M_x}^{N_x} \mathbf{c}_j{}^{n+1} \left[\frac{d^2S(j,h)\circ\phi(x)}{d\phi(x)^2}\left(\frac{d\phi(x)}{dx}\right)^2 + \frac{dS(j,h)\circ\phi(x)}{d\phi(x)}\ \frac{d^2\phi(x)}{dx^2}\right]. \tag{35}$$

B. Formulating the Discrete System

Define A_{jk} and B_{jk} as $m \times m$ matrices

$$\begin{aligned} A_{jk} &= \frac{\delta_{jk}^{(2)}}{h^2}(\phi'(x_k))^2 + \frac{\delta_{jk}^{(1)}}{h}\phi''(x_k), \\ B_{jk} &= \frac{\delta_{jk}^{(1)}}{h}\phi'(x_k), \text{ and} \\ I^{(0)} &= [\delta_{jk}^{(0)}]. \end{aligned} \tag{36}$$

Note that these may be expressed in matrix notation, using (25), as

$$\begin{aligned} A &= \frac{1}{h^2}\operatorname{diag}\left((\phi')^2\right) I_{m\times m}^{(2)} + \frac{1}{h}\operatorname{diag}\left(\phi''\right) I_{m\times m}^{(1)}, \\ B &= \frac{1}{h}\operatorname{diag}(\phi'(x)) I_{m\times m}^{(1)}, \text{ and} \\ I &= I_{m\times m}^{(0)}. \end{aligned} \tag{37}$$

We evaluate the discrete solution $\mathbf{U}^{n+1}$ and its derivatives at collocation points x_k for $k = -M_x, \ldots, N_x$ in the spatial variable, to obtain

$$\mathbf{U}^{n+1}(x_k) = \sum_{j=-M_x}^{N_x} \mathbf{c}_j{}^{n+1}\delta_{jk}^{(0)} = (IC^{n+1})_k, \tag{38}$$

$$\mathbf{U}_x^{n+1}(x_k) = \sum_{j=-M_x}^{N_x} \mathbf{c}_j{}^{n+1}\frac{\delta_{jk}^{(1)}}{h}\phi'(x_k) = (BC^{n+1})_k, \tag{39}$$

$$\begin{aligned} \mathbf{U}_{xx}^{n+1}(x_k) &= \sum_{j=-M_x}^{N_x} c_j^{n+1}\left(\frac{\delta_{jk}^{(2)}}{h^2}(\phi'(x_k))^2 + \frac{\delta_{jk}^{(1)}}{h}\phi''(x_k)\right) \\ &= (AC^{n+1})_k. \end{aligned} \tag{40}$$

VI. Fully Discretized System

Substituting (38), (39), and (40) into (29), with I and A as defined in (37), we obtain

$$\begin{aligned} &(IC^{n+1})_k - \Delta t\theta(AC^{n+1})_k\mathbf{D} = (IC^n)_k \\ &+ \Delta t(1-\theta)(AC^n)_k\mathbf{D} + \Delta t\mathbf{Q}(x_k, t^n, \mathbf{U}^n, \mathbf{U}_x^n), \end{aligned} \tag{41}$$

which can be rewritten as

$$\begin{aligned} &\left((I - \Delta t\theta A\mathbf{D})\, C^{n+1}\right)_k = \left((I + \Delta t(1-\theta)A\mathbf{D})\, C^n\right)_k \\ &+ \Delta t\mathbf{Q}(x_k, t^n, \mathbf{U}^n, \mathbf{U}_x^n). \end{aligned} \tag{42}$$

Equation (42) can be represented as μ different $m \times m$ linear systems that can be solved independently,

$$\begin{aligned} (I - \Delta t\theta AD_i)\, C_i^{n+1} &= (I + \Delta t(1-\theta)AD_i)\, C_i^n \\ &+ \Delta t Q_i(\mathbf{x^n}, t^n, \mathbf{U}^n, \mathbf{U}_x^n), \end{aligned} \tag{43}$$

where D_i is a diagonal diffusion coefficient matrix. This formulation allows for efficient computation of each component while retaining the coupling between different variables through Q_i.

A. Linear Stability Analysis

Ignoring the nonlinear term Q_i, the iteration (43) reduces to the repeated application of the iteration matrix

$$(I - \Delta t\theta AD_i)^{-1}(I + \Delta t(1-\theta)AD_i)\ .$$

If the spectral radius of this matrix exceeds 1, then the iteration is unstable. If A has an eigenvector with eigenvalue λ, then this iteration matrix has the same eigenvector with eigenvalue

$$\frac{1 + \Delta t(1-\theta)D\lambda}{1 - \Delta t\theta D\lambda}\,. \tag{44}$$

For Euler's method, which has $\theta = 0$, the requirement for stability becomes $|1 + \Delta t D\lambda| \le 1$. In the classical finite-differences case [30], the bound $-\Delta x^{-2} < \lambda \le 0$ leads to the usual requirement that $\Delta t \le \Delta x^2/(2D)$. For the Sinc differentiation matrix $I^{(2)}$ itself, the eigenvalues satisfy $-\pi^2 < \lambda \le 0$ [22, P.151], which would lead to a similar requirement that $\Delta t \le 2\Delta x^2/(\pi^2 D)$. However, the SE and DE conformal maps concentrate points near the ends of the interval, leading effectively to very small Δx, and eigenvalues that grow rapidly with m. Consequently, Δt must be so small that the approach is not worthwhile.

In contrast, if $\theta \in [1/2, 1]$, such as the classical C-N case of $\theta = 1/2$, then the expression (44) has absolute value at most one for any $\lambda \le 0$. Consequently, within the C-N method, the rapid growth of eigenvalues of A does not cause a problem.

VII. Numerical Solution

A. Measures of Error

We define the metrics used to evaluate the errors of our numerical solutions $\mathbf{U}(x,t)$ with respect to exact solutions $\mathbf{u}(x,t)$. The pointwise absolute error at a specific grid point x_k, time step t_j, and component $i = 1, 2, \ldots, \mu$ is defined

$$e(i,k,j) = \left| u_i(x_k,t_j) - U_i(x_k,t_j) \right|.$$

The L_∞ error over all spatial grid points and at the final time step for a single component i is defined as

$$E_{\infty,i}(T) = \max_{-M_x \le k \le N_x} e(i,k,N). \tag{45}$$

The L^2 error is calculated using the trapezoidal rule to approximate the integral of the squared error over the spatial domain for specific time t_j and component i. So, we compute $E_2(i,j) =$

$$\left(\sum_{k=-M_x}^{N_x-1} (x_{k+1} - x_k) \frac{e(i,k,j)^2 + e(i,k+1,j)^2}{2} \right)^{1/2}. \tag{46}$$

This method accounts for uneven spacing between the collocation points.

In [10] errors were calculated at collocation points $\{x_k\}$ only. However, the Sinc series solution can be evaluated at any x. In this paper we will not only evaluate the errors at the collocation points, but also at "interpolation points" in between collocation points. For each method we will place 3 interpolation points between each pair of collocation points. For the Sinc-Hybrid method the collocation points are evenly spaced and so we place the interpolation points with even spacing. For our method we place interpolation points evenly in the transformed variable, then transform them back to the original variable by ϕ^{-1}. That is, for SE by equation (16), and for DE by (18). Specifically, we set $\hat{x}_p = \phi^{-1}(ph/4)$, for $p = -4M_x - 3, \ldots, 4N_x + 3$.

B. Convergence Order

The empirical convergence order P_i for each component of the vector $\mathbf{U}(x,t)$ is calculated by

$$P_i = \frac{\log(E_m^{U_i} / E_{2m}^{U_i})}{\log\left(\frac{1}{m} \middle/ \frac{1}{2m} \right)}, \quad i = 1, 2, \ldots, \mu,$$

where $E_m^{U_i}$ represents the error for the i-th component using m collocation points.

The transformations defined in Equations (14) and (17) are used for all examples. In all of our examples, we will choose a symmetric gird, so $M_x = N_x$. According to Theorem 3.1 from [27] or Theorem 3.4 from [22] we compute

$$h_S = \left(\frac{\pi d}{\alpha N_x} \right)^{1/2},$$

where d is the width of the strip in (13) and α is the rate of decay of f at $\pm\infty$. For the SE transformation and a differentiable function f with $f(a) = 0$ and $f'(a) \neq 0$ one can show directly that $\alpha = 1$. Following [22], $d \le \pi/2$ and so we choose $d = \pi/2$.

For the DE transformation, based on Theorem 3.2 in [27] and [31], we set

$$h_D = \frac{\ln(\pi d \gamma N_x / \delta)}{\gamma N_x},$$

where d is the width of the strip in (13), and δ and γ depend on the decay of f. An analysis of the parameters to use for different examples was given in [32]. Here, after some preliminary tests, we chose $d = 1/2$, $\delta = 2/\pi$, and $\gamma = 2$.

The linear systems in (29) and (31) can become ill-conditioned. Therefore, we apply left-diagonal preconditioning when solving them.

C. Numerical Solution of Burgers' Equation

We will test our method on the examples found in [10] and compare with results for the Sinc-Hybrid method as well as a few other methods.

Example 1. We first consider the example found in [10] and [16], which is given by

$$u_t = D u_{xx} - u u_x, \quad 0 < x < 1, \quad 0 < t \le 1,$$
$$u(x,0) = \frac{2D\pi \sin(\pi x)}{2 + \cos(\pi x)},$$
$$u(0,t) = 0, \quad u(1,t) = 0,$$

for which the exact solution is given by:

$$u(x,t) = \frac{2D\pi e^{-\pi^2 Dt} \sin(\pi x)}{2 + e^{-\pi^2 Dt} \cos(\pi x)}.$$

Using the numerical scheme from Section V, we set $\theta = \frac{1}{2}$. Figure 3 plots the numerical solution using SCM-DE at interpolation points, as described in (43).

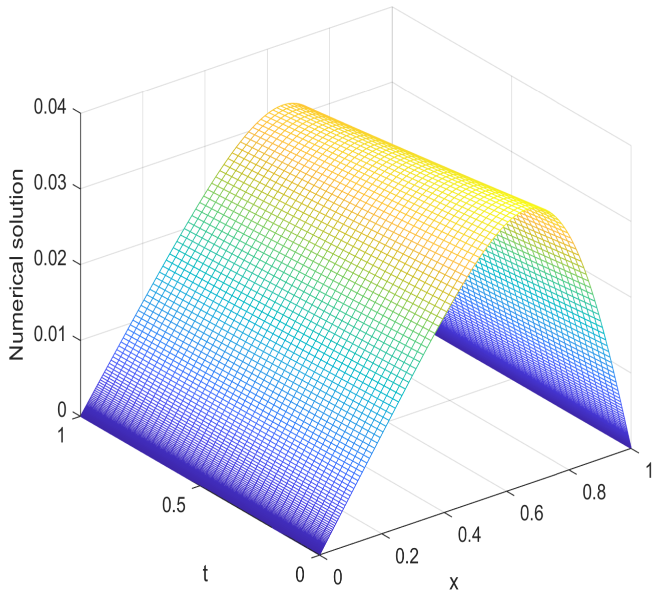

Fig. 3: Numerical solution using SCM-DE at interpolation points for Example 1 with parameters $T = 1$, $m + 1 = 80$, $L = 1.00$, $N = 40$, $D = 0.01$, and $\theta = 1/2$. The exact solution is visually indistinguishable.

To compare with [10], we set $D = 0.01$ and $\Delta t = (m+1)^{-2}$. Maximum absolute errors $E_\infty(T)$ at $T = 1$ for various $m+1$ values were computed for both collocation and interpolation points using Euler's and Heun's methods under SE and DE transformations. Comparisons were made with the Hybrid method from [10], and for collocation points, also with the standard second-order Crank–Nicolson Finite Difference (CN-FD) method. Tables I and II illustrate SCM's accuracy, particularly with SCM-DE and Heun's method.

Figures 4a and 4b compare errors for SCM-DE and Hybrid methods at collocation and interpolation points. The SCM-DE method achieves consistent error magnitudes, around 10^{-11}, at both collocation and interpolation points. In contrast, the Hybrid method shows oscillatory error behavior with larger magnitudes, approximately 10^{-4}, indicating Runge's phenomenon between collocation points.

Tables III and IV present the maximum absolute error E_∞ and L^2 error, respectively, at $T = 1$ for various $m + 1$ collocation points across decreasing time steps Δt. The observed error decay with increasing $m + 1$ and decreasing Δt confirms the SCM-DE method's stability and convergence.

Figure 5 presents log plots of the maximum absolute errors, $E_\infty(T)$, data from Table III, as functions of the time step size, Δt, and the number of intervals, $m + 1$. The empirical convergence orders P in Table V indicate that the SCM-DE method achieves high-order spatial accuracy, approaching order 8.63 as $m + 1$ increases. Table VI also shows stable second-order time convergence across refined Δt values, affirming the SCM-DE method's robustness and accuracy in both space and time. Similar results were obtained using the L^2 norm.

TABLE I: Maximum absolute errors $E_\infty(T)$ measured at collocation points at $T = 1$ for Example 1 with parameters from [10], for various number of intervals $m + 1$. Here, $L = 1$, $D = 0.01$, $\theta = \frac{1}{2}$, and $\Delta t = (\frac{1}{m+1})^2$. SCM-DE with Heun's method significantly outperforms the other methods.

Intervals	SCM				Hybrid [10]	CN-FD
	Euler's method		Heun's method			
$m+1$	DE	SE	DE	SE		
10	3.829×10^{-4}	7.673×10^{-4}	3.828×10^{-4}	7.675×10^{-4}	3.073×10^{-4}	2.267×10^{-4}
20	1.950×10^{-6}	1.063×10^{-4}	1.953×10^{-6}	1.063×10^{-4}	6.929×10^{-5}	5.910×10^{-5}
40	1.524×10^{-7}	6.831×10^{-6}	7.314×10^{-9}	6.831×10^{-6}	1.579×10^{-5}	1.487×10^{-5}
80	3.855×10^{-8}	1.200×10^{-7}	1.676×10^{-11}	1.200×10^{-7}	3.834×10^{-6}	3.730×10^{-6}
160	9.754×10^{-9}	9.530×10^{-9}	3.694×10^{-14}	3.727×10^{-10}	9.406×10^{-7}	9.325×10^{-7}

TABLE II: Maximum absolute errors $E_\infty(T)$ measured at interpolation points at $T = 1$ for Example 1 with parameters from [10], for various number of intervals $m + 1$. Here, $L = 1$, $D = 0.01$, $\theta = \frac{1}{2}$, and $\Delta t = (\frac{1}{m+1})^2$. Comparing with Table I, we see that for SCM the errors at interpolation points are similar to the errors at collocation points. In contrast, for the Sinc-Hybrid method the errors at interpolation points are significantly larger than at collocation points in Table I.

Intervals	SCM				Hybrid [10]
	Euler's method		Heun's method		
$m+1$	DE	SE	DE	SE	
10	5.210×10^{-4}	8.787×10^{-4}	5.220×10^{-4}	8.788×10^{-4}	1.264×10^{-3}
20	6.492×10^{-6}	1.110×10^{-4}	6.629×10^{-6}	1.111×10^{-4}	7.055×10^{-4}
40	1.524×10^{-7}	7.550×10^{-6}	8.823×10^{-9}	7.550×10^{-6}	3.648×10^{-4}
80	3.902×10^{-8}	1.228×10^{-7}	1.683×10^{-11}	1.228×10^{-7}	1.844×10^{-4}
160	9.756×10^{-9}	9.625×10^{-9}	3.687×10^{-14}	3.742×10^{-10}	9.257×10^{-5}

TABLE III: Maximum absolute errors $E_\infty(T)$ using SCM-DE measured at collocation points at $T = 1$ for Example 1 with parameters from [10]. Here, $L = 1$, $D = 0.01$, and $\theta = \frac{1}{2}$. The number of intervals is $m + 1 = 2N_x + 2$.

Δt	$m+1=10$	$m+1=20$	$m+1=40$	$m+1=80$	$m+1=160$
10^{-1}	2.362×10^{-4}	2.610×10^{-6}	4.287×10^{-7}	4.313×10^{-7}	4.313×10^{-7}
10^{-2}	3.828×10^{-4}	2.274×10^{-6}	7.465×10^{-9}	4.453×10^{-9}	4.454×10^{-9}
10^{-3}	3.828×10^{-4}	1.371×10^{-6}	7.363×10^{-9}	4.576×10^{-11}	4.468×10^{-11}
10^{-4}	3.828×10^{-4}	1.557×10^{-6}	7.450×10^{-9}	1.711×10^{-11}	4.764×10^{-13}
10^{-5}	3.828×10^{-4}	1.557×10^{-6}	7.621×10^{-9}	1.721×10^{-11}	2.992×10^{-13}

TABLE IV: Error $E_2(T)$ at $T = 1$ for Example 1 using SCM-DE at collocation points with $T = 1.00$, $L = 1.00$, $D = 0.01$, and $\theta = \frac{1}{2}$.

Δt	$m+1=10$	$m+1=20$	$m+1=40$	$m+1=80$	$m+1=160$
10^{-1}	1.070×10^{-4}	6.090×10^{-7}	1.883×10^{-7}	1.881×10^{-7}	1.882×10^{-7}
10^{-2}	1.112×10^{-4}	5.254×10^{-7}	3.012×10^{-9}	1.929×10^{-9}	1.929×10^{-9}
10^{-3}	1.112×10^{-4}	5.244×10^{-7}	1.947×10^{-9}	2.086×10^{-11}	1.934×10^{-11}
10^{-4}	1.112×10^{-4}	5.244×10^{-7}	1.943×10^{-9}	4.651×10^{-12}	2.087×10^{-13}
10^{-5}	1.112×10^{-4}	5.244×10^{-7}	1.943×10^{-9}	4.647×10^{-12}	9.273×10^{-14}

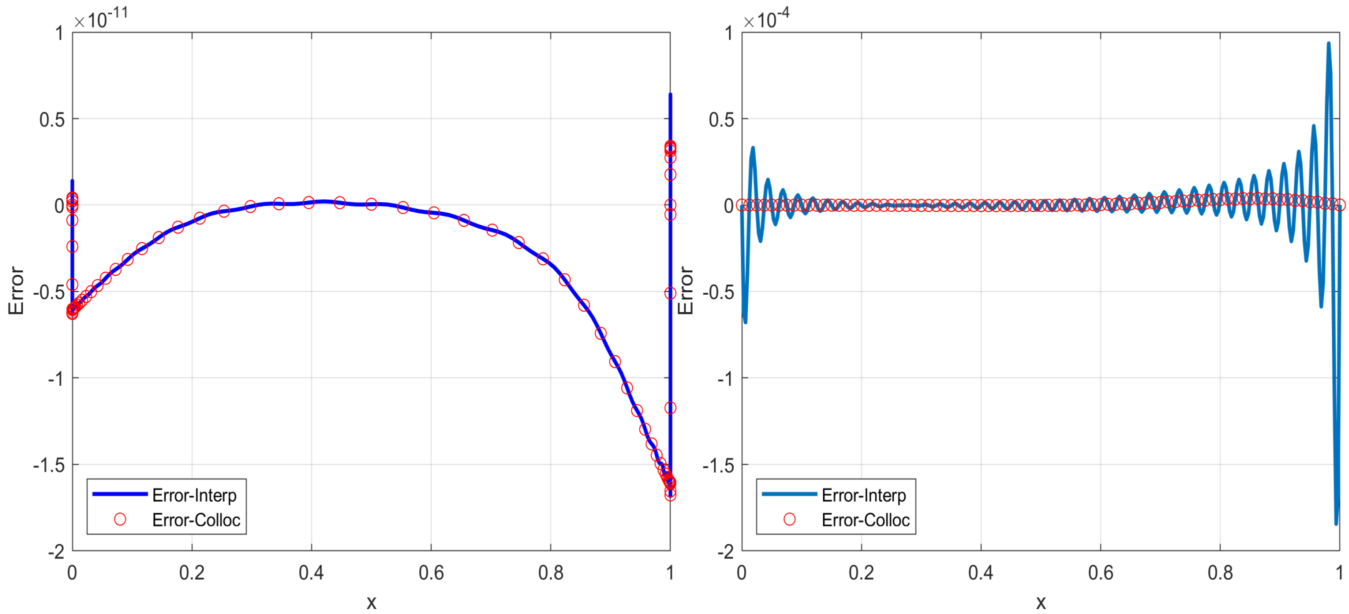

(a) SCM-DE error

(b) Sinc-Hybrid error

Fig. 4: Error plots at $T = 1$ for Example 1 with parameters from [10], with $L = 1$, $D = 0.01$, $\theta = \frac{1}{2}$, $m + 1 = 80$ and $\Delta t = (\frac{1}{m+1})^2$. Markers represent collocation points and curves represent the Sinc interpolation. These figures illustrate that the Sinc-Hybrid method suffers from Runge's phenomenon, while the SCM-DE method does not.

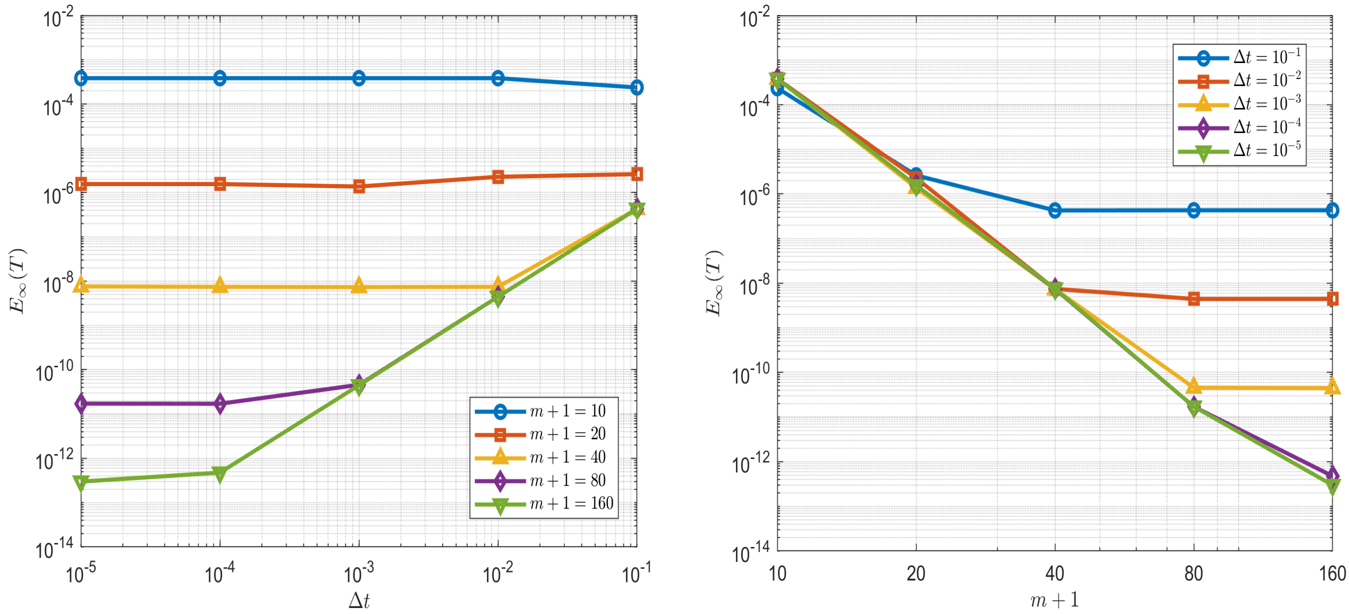

(a) Error vs time step Δt

(b) Error vs number of intervals $m + 1$

Fig. 5: Maximum absolute errors for Example 1 using the data from Table III. (Left) Log plot of $E_\infty(T)$ vs Δt for different values of $m + 1$. (Right) Semi-log plot of $E_\infty(T)$ vs number of intervals $m + 1$ for different Δt. The right plot appears linear, indicating exponential convergence.

TABLE V: Empirical convergence orders P in the spatial variable for various Δt using the L_∞ norm with SCM-DE from Table III for Example 1. Orders up to 8.63 are observed. As one goes across a row, the time error associated with Δt eventually dominates, and the order with respect to $m + 1$ is no longer observable.

Δt	$m+1=10$	$m+1=20$	$m+1=40$	$m+1=80$	$m+1=160$
10^{-1}	–	6.03	2.51	−0.01	0.00
10^{-2}	–	6.86	7.95	0.73	0.00
10^{-3}	–	7.54	7.27	7.20	0.03
10^{-4}	–	7.37	7.43	8.61	5.12
10^{-5}	–	7.37	7.40	8.63	5.79

TABLE VI: Empirical convergence orders P in the time variable for each $m+1$ value using the L_∞ norm with SCM-DE from Table III for Example 1. Orders up to 2 are observed. As one goes down a column, the error due to $m+1$ eventually dominates, and the order with respect to Δt is no longer observable.

Δt	$m+1=10$	$m+1=20$	$m+1=40$	$m+1=80$	$m+1=160$
10^{-1}	–	–	–	–	–
10^{-2}	-0.21	0.06	1.76	1.99	1.99
10^{-3}	0.00	0.22	0.01	1.99	2.00
10^{-4}	0.00	-0.06	-0.01	0.43	1.97
10^{-5}	0.00	0.00	-0.01	0.00	0.20

Example 2. We consider the example found in [16], which is similar to Example 1, except that the parameters A and D will vary.

$$u_t = Du_{xx} - uu_x, \quad 0 < x < 1, \quad t > 0,$$
$$u(x,0) = \frac{2D\pi \sin(\pi x)}{A + \cos(\pi x)}, \quad A > 1.$$
$$u(0,t) = 0, \quad u(1,t) = 0,$$

for which the exact solution is given by:

$$u(x,t) = \frac{2D\pi e^{-\pi^2 Dt} \sin(\pi x)}{A + e^{-\pi^2 Dt} \cos(\pi x)}.$$

Using the numerical scheme from Section V, we set $\theta = \frac{1}{2}$. Figure 6 plots the numerical solution using SCM-DE at collocation and interpolation points, as described in (43).

To compare with the Milne method from [16], we set $L = 1$, $D = 0.001$, $A = 1.1$, and $\Delta t = 10^{-2}$. Since D is small, the equation can be considered as a singular perturbation problem. Maximum absolute errors $E_\infty(T)$ at $T = 1$ for various $m+1$ values were computed for both collocation and interpolation points using our numerical approach. Table VII illustrates that SCM-DE with Heun's method has superior accuracy.

Figure 7 illustrates the final-time solution $u(x,T)$ obtained using the SCM-DE method. Subfigure 7a compares the effect of varying the diffusion coefficient D while keeping $A = 1.1$ fixed, showing that lower diffusion coefficients yield smoother and more uniform solution curves. Subfigure 7b explores the impact of different A values with fixed $D = 0.001$, indicating that increasing A reduces the solution's peak magnitude. In both cases, the numerical solutions closely match the exact solutions, confirming the accuracy and stability of the proposed method.

Table VIII provides a comparison of the L_2-norm errors obtained using the proposed SCM-DE method at collocation points and the results reported in [16]. The comparison is conducted for various values of the nonlinearity parameter A and diffusion coefficient $\mu = D$, with two different time step sizes, $\Delta t = 0.01$ and $\Delta t = 0.001$. The results clearly demonstrate the improved accuracy of the SCM-DE method across all tested configurations, especially for smaller diffusion coefficients and coarser time steps, highlighting its effectiveness in solving nonlinear parabolic problems.

Table IX shows the maximum absolute error E_∞ at $T = 1$, with $A = 1.1$, for various $m+1$ intervals and decreasing time steps Δt, confirming the stability and convergence of the SCM-DE method. Notably, SCM-DE avoids Runge's phenomenon for this nearly singular problem. We also conducted tests with $\theta = 1$, which showed slightly higher errors compared to $\theta = 0.5$, though the errors remained within the same order of convergence and were still of comparable magnitude.

In Figure 8, we plot the absolute errors at collocation and interpolation points for the SCM-DE method, using parameters from [16] with $m+1 = 160$, $L = 1.00$, $D = 0.001$, $\theta = \frac{1}{2}$, $A = 1.1$ and $\Delta t = 10^{-3}$.

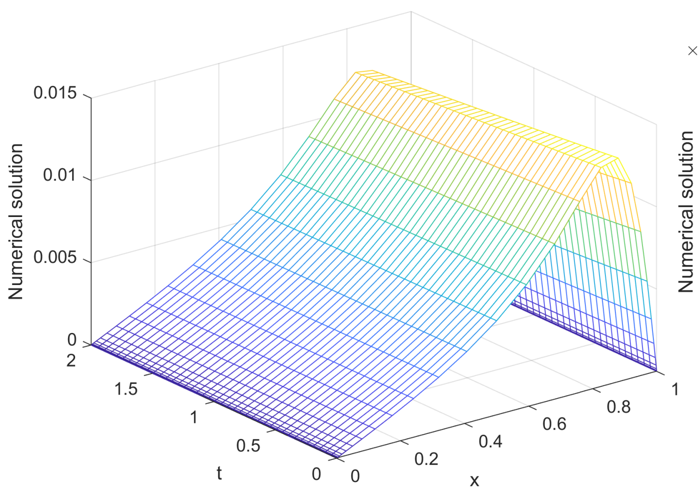

(a) At Collocation Points

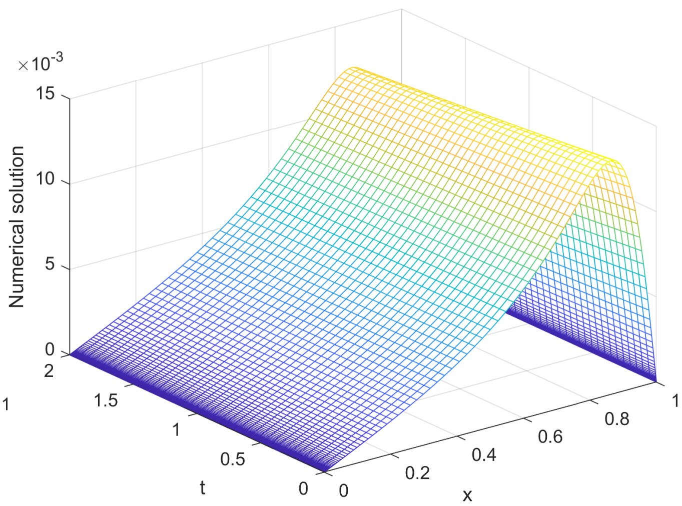

(b) At Interpolation Points

Fig. 6: Numerical solutions using SCM-DE at Collocation and Interpolation points for Example 2 with parameters from [16]. Here, $m+1 = 40$ with $L = 1.00$, $D = 0.001$, $A = 1.1$, $\theta = \frac{1}{2}$, and $\Delta t = 0.05$.

TABLE VII: Comparison of $E_\infty(T)$ and $E_2(T)$ errors at $T = 1$ for Example 2 with parameters from [16] using SCM-DE with Heun's method and the Milne method at different values of $m + 1$. Here, $L = 1$, $D = 0.001$, $A = 1.1$ $\theta = \frac{1}{2}$, and $\Delta t = 10^{-2}$.

Intervals	SCM-DE with Heun's method				Milne Method [16]	
	Collocation Points		Interpolation Points			
$m+1$	$E_\infty(T)$	$E_2(T)$	$E_\infty(T)$	$E_2(T)$	$E_\infty(T)$	$E_2(T)$
10	2.2985×10^{-4}	3.4747×10^{-5}	5.7934×10^{-4}	2.1031×10^{-4}	3.7899×10^{-4}	3.8091×10^{-4}
20	1.9218×10^{-5}	4.1196×10^{-6}	3.2335×10^{-5}	9.0310×10^{-6}	1.4753×10^{-4}	1.8308×10^{-4}
40	3.5308×10^{-8}	1.5182×10^{-8}	1.3317×10^{-7}	6.5859×10^{-8}	3.8173×10^{-5}	6.6726×10^{-5}
80	8.0330×10^{-10}	1.9741×10^{-10}	8.0330×10^{-10}	1.9727×10^{-10}	9.6834×10^{-6}	2.3750×10^{-5}
160	8.0394×10^{-10}	1.9709×10^{-10}	8.0394×10^{-10}	1.9702×10^{-10}	9.6834×10^{-6}	2.3750×10^{-5}

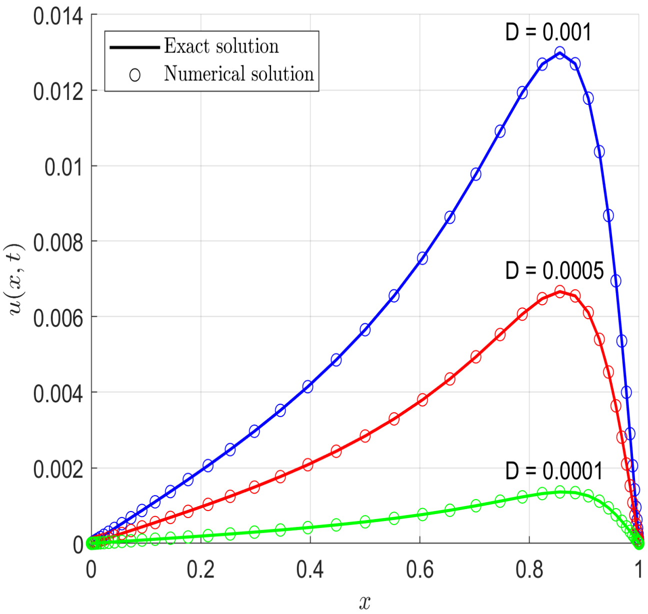

(a) Final-time for different values of D at collocation points with fixed $A = 1.1$.

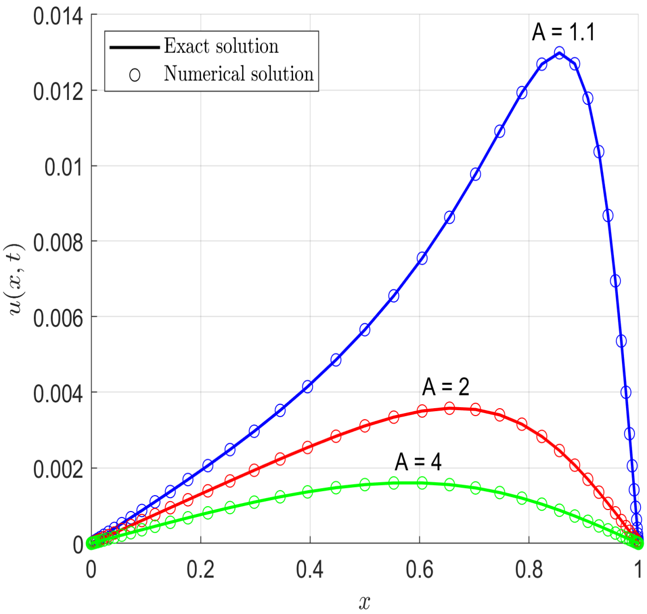

(b) Final-time for different values of A at collocation points with fixed $D = 0.001$.

Fig. 7: Comparison of numerical and exact solutions at final time $T = 1$ for Example 2 using SCM-DE for various values of (a) D and (b) A. The numerical results are computed at collocation points using $m + 1 = 80$, $\theta = 0.5$, and $\Delta t = 0.01$.

TABLE VIII: Comparison of L_2-norm errors for different values of A and $\mu = D$ in Example 2, using SCM-DE and the method from Milne Paper [16], with $\Delta t = 0.01$ and $\Delta t = 0.001$.

Δt	D	$A = 1.1$		$A = 2$		$A = 4$	
		SCM-DE	[16]	SCM-DE	[16]	SCM-DE	[16]
0.010	0.0010	1.97×10^{-10}	2.38×10^{-5}	4.19×10^{-13}	2.25×10^{-7}	1.11×10^{-13}	3.03×10^{-8}
0.010	0.0005	1.56×10^{-11}	6.87×10^{-6}	1.24×10^{-13}	5.76×10^{-8}	4.60×10^{-14}	7.67×10^{-9}
0.010	0.0001	1.65×10^{-13}	3.12×10^{-7}	1.68×10^{-14}	2.35×10^{-9}	6.18×10^{-15}	3.10×10^{-10}
0.001	0.0010	3.35×10^{-12}	2.37×10^{-5}	2.94×10^{-13}	2.25×10^{-7}	1.09×10^{-13}	3.03×10^{-8}
0.001	0.0005	1.16×10^{-12}	6.87×10^{-6}	1.25×10^{-13}	5.76×10^{-8}	4.61×10^{-14}	7.67×10^{-9}
0.001	0.0001	1.68×10^{-13}	3.12×10^{-7}	1.68×10^{-14}	2.35×10^{-9}	6.20×10^{-15}	3.10×10^{-10}

TABLE IX: Maximum absolute errors $E_\infty(T)$ using SCM-DE with Heun's method measured at collocation points at $T = 1$ for Example 2. Here, $L = 1$, $D = 0.001$, and $\theta = \frac{1}{2}$.

Δt	$m+1=10$	$m+1=20$	$m+1=40$	$m+1=80$	$m+1=160$
10^{-1}	1.641×10^{-4}	1.324×10^{-5}	1.009×10^{-7}	7.799×10^{-8}	7.804×10^{-8}
10^{-2}	2.298×10^{-4}	1.922×10^{-5}	3.531×10^{-8}	8.033×10^{-10}	8.039×10^{-10}
10^{-3}	2.298×10^{-4}	2.244×10^{-5}	3.724×10^{-8}	1.788×10^{-11}	8.063×10^{-12}
10^{-4}	2.298×10^{-4}	2.245×10^{-5}	3.972×10^{-8}	1.723×10^{-11}	6.929×10^{-14}
10^{-5}	2.298×10^{-4}	2.245×10^{-5}	4.391×10^{-8}	1.748×10^{-11}	1.469×10^{-13}

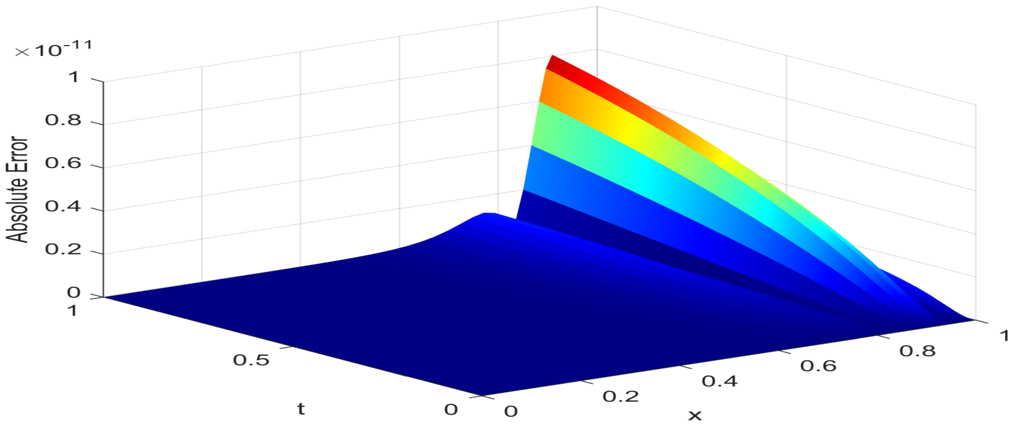

(a) At Collocation Points

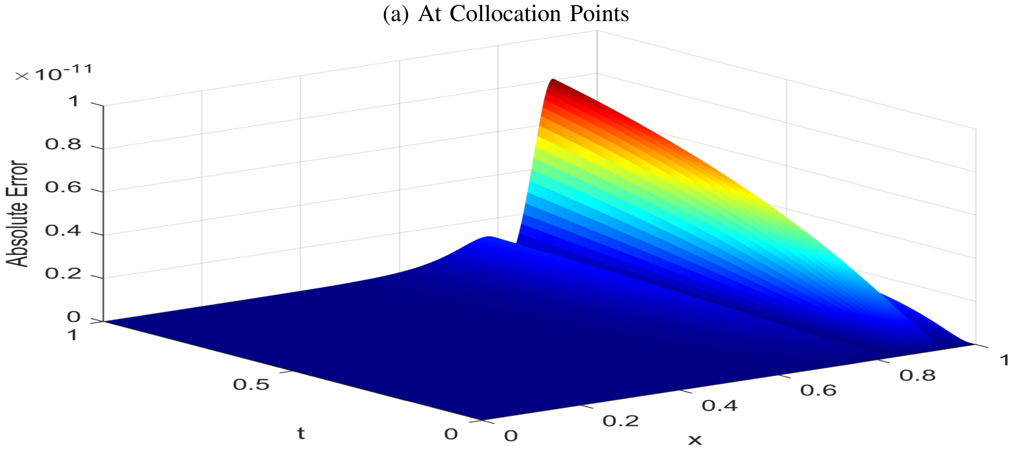

(b) At Interpolation Points

Fig. 8: Absolute errors for SCM-DE at Collocation and Interpolation points for Example 2 with parameters from [16]. Here, $m+1=160$ with $L=1.00$, $D=0.001$, $\theta=\frac{1}{2}$, $A=1.1$, and $\Delta t=10^{-3}$. For SCM-DE applied to this nearly singular problem, we do not observe Runge's phenomenon.

Example 3. In this example, we consider the following Burgers' equation [10]:

$$u_t + uu_x = u_{xx}, \quad 0 < x < 1, \quad 0 < t \leq 1,$$

$$u(x,0) = f(x),$$

$$u(0,t) = u(1,t) = 0.$$

The initial value $f(x)$ has two cases:

$$f(x) = \sin(\pi x) \quad \text{or} \quad f(x) = 4x(1-x).$$

We set intervals, $m+1=80$, and $\Delta t = 10^{-5}$ for our numerical experiments. The results, shown in Tables X and XI, compare the exact solutions, calculated using Fourier series [33], and numerical solutions for Example 3 with different initial conditions. Tables X and XI present comparisons for $f(x) = \sin(\pi x)$ and $f(x) = 4x(1-x)$, respectively. In both cases, the Sinc-DE method with $\theta = \frac{1}{2}$ matches the exact solution to at least 6 significant digits, significantly outperforming the Hybrid method in [10]. Separate tests again confirm that the C-N method $\theta = 1/2$ is slightly more accurate than the fully implicit method $\theta = 1$.

TABLE X: Exact solutions and numerical solutions for Example 3 when $\varphi(x) = \sin(\pi x)$, with $m+1=80$ and $\Delta t = 10^{-5}$. Note that the Sinc-DE with Crank-Nicholson method gives the exact solution (from Fourier series) to at least 6 decimal places.

x	t	Sinc-DE		[10]		Exact solution
		$\theta=\frac{1}{2}$	$\theta=1$	$\theta=\frac{1}{2}$	$\theta=1$	
0.25	0.1	0.253638	0.253649	0.253665	0.253679	0.253638
0.25	0.15	0.156601	0.156612	0.156628	0.156640	0.156601
0.25	0.2	0.096442	0.096451	0.096465	0.096475	0.096442
0.25	0.25	0.059218	0.059225	0.059236	0.059243	0.059218
0.5	0.1	0.371577	0.371596	0.371625	0.371644	0.371577
0.5	0.15	0.226824	0.226840	0.226867	0.226884	0.226824
0.5	0.2	0.138473	0.138487	0.138509	0.138523	0.138473
0.5	0.25	0.084538	0.084548	0.084565	0.084575	0.084538
0.75	0.1	0.272582	0.272596	0.272623	0.272635	0.272582
0.75	0.15	0.164369	0.164382	0.164404	0.164416	0.164369
0.75	0.2	0.099435	0.099445	0.099462	0.099472	0.099435
0.75	0.25	0.060347	0.060355	0.060367	0.060375	0.060347

TABLE XI: Exact solutions and numerical solutions for Example 3 when $\varphi(x) = 4x(1-x)$, with $m+1 = 80$ and $\Delta t = 10^{-5}$. The Sinc-DE with C-N method matches the exact solution (from Fourier series) to at least 6 decimal places.

x	t	Sinc-DE		[10]		Exact solution
		$\theta=\frac{1}{2}$	$\theta=1$	$\theta=\frac{1}{2}$	$\theta=1$	
0.25	0.01	0.66006	0.66007	0.66008	0.66009	0.66006
0.25	0.05	0.42629	0.42630	0.42631	0.42632	0.42629
0.25	0.10	0.26148	0.26149	0.26151	0.26152	0.26148
0.25	0.15	0.16148	0.16149	0.16150	0.16152	0.16148
0.25	0.25	0.06109	0.06109	0.06111	0.06111	0.06109
0.5	0.01	0.91972	0.91972	0.91972	0.91972	0.91972
0.5	0.05	0.62808	0.62810	0.62812	0.62814	0.62808
0.5	0.10	0.38342	0.38344	0.38347	0.38349	0.38342
0.5	0.15	0.23406	0.23407	0.23410	0.23412	0.23406
0.5	0.25	0.08723	0.08724	0.08726	0.08727	0.08723
0.75	0.01	0.68364	0.68364	0.68365	0.68366	0.68364
0.75	0.05	0.46525	0.46526	0.46529	0.46530	0.46525
0.75	0.10	0.28157	0.28159	0.28161	0.28163	0.28157
0.75	0.15	0.16974	0.16975	0.16977	0.16979	0.16974
0.75	0.25	0.06229	0.06230	0.06231	0.06232	0.06229

Example 4. We also consider the coupled Burgers' equation discussed in [10]. Specifically, we consider the following coupled equations along with initial and homogeneous boundary conditions. For $0 < x < 2\pi,\ 0 < t \le T$,

$$u_t = u_{xx} + 2uu_x - (uv)_x,$$
$$v_t = v_{xx} + 2vv_x - (uv)_x,$$
$$u(x,0) = v(x,0) = \sin(x-\pi),$$
$$u(0,t) = u(2\pi,t) = v(0,t) = v(2\pi,t) = 0.$$

The exact solution is

$$u(x,t) = v(x,t) = e^{-t}\sin(x-\pi).$$

Figure 9 plots the numerical solution using SCM-DE at interpolation points, as described in (43).

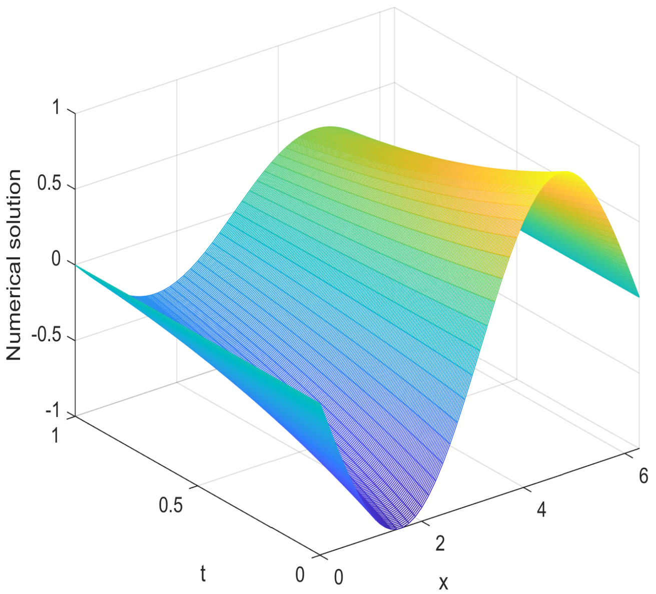

Fig. 9: Numerical solution using SCM-DE at interpolation points for Example 4 with parameters $T = 1$, $m+1 = 64$, $L = 2\pi$, $N = 200$, and $\theta = \frac{1}{2}$. The exact solution is visually indistinguishable.

Tables XII and XIII present maximum absolute errors for Example 4 with $N = 1000$ and $\theta = \frac{1}{2}$, comparing SCM-DE accuracy against the method in [10] at $T = 0.1$ and $T = 0.5$ for both collocation and interpolation points.

Table XIV shows the maximum $L_\infty(T)$ errors at collocation points for Example 4, with SCM-DE parameters $T = 0.10$, $L = 2\pi$, and $\theta = \frac{1}{2}$. We also calculated the empirical convergence orders, which are similar to those in Example 1. In other words, the method again achieves exceptionally high accuracy, with 2nd order convergence in time and higher order in space.

Figures 10a and 10b illustrate error comparisons for both SCM-DE and Hybrid methods at collocation and interpolation points, underscoring the accuracy of each method for solving Example 4.

On these coupled equations, the method produces very high order approximations and a significant increase in accuracy over the Sinc-Hybrid method. Note that the error at the interpolation points indicate again that the Sinc-Hybrid method is susceptible to Runge's phenomenon while the SCM-DE is not.

In addition, we also investigated a variation of Example 4 that has been widely studied [34], [35], [11]. In particular, we take

$$u(x,0) = \begin{cases} \sin(2\pi x), & x \in [0, 0.5], \\ 0, & x \in (0.5, 1], \end{cases} \tag{5.9}$$

$$v(x,0) = \begin{cases} 0, & x \in [0, 0.5], \\ -\sin(2\pi x), & x \in (0.5, 1], \end{cases} \tag{5.10}$$

and zero boundary conditions. This initial condition is non-smooth. The standard theory of convergence for sinc collocation only applies to analytic functions. We observe that the results of the Sinc-DE method are not as accurate as for the previous examples. We see in Figure 11 that the Sinc-DE solution oscillates in x for t near 0. This illustrates that the Sinc-DE method is not ideal for problems with non-smooth initial conditions.

Tables XVI and XVII present the maximum absolute errors for $u(x,t)$ and $v(x,t)$, respectively, in Example 4 at different values of T and $m+1$. Since an exact solution is unavailable, the errors are measured relative to the numerical solutions computed with $m+1 = 160$. The results indicate that while the SCM-DE method is stable and fairly accurate for this non-smooth initial condition, it does not achieve the exceptionally high order or accuracy as for smooth problems.

Table XV shows the approximate maximum values of u and v at different time levels for Example 4, using data from [34]. The parameters are $L = 1$, $m + 1 = 50$, $\theta = \frac{1}{2}$, $\Delta t = 10^{-5}$, $D_1 = D_2 = 1$, $\eta = \xi = 2$, and $\alpha = \beta = 10$, with non-symmetric, non-smooth initial conditions.

TABLE XII: The maximum absolute error at collocation points for the coupled equations in Example 4, with $L = 2\pi$, $\theta = \frac{1}{2}$ and $N = 1000$.

$m+1$	$T = 0.1$		$T = 0.5$	
	Sinc-DE	[10]	Sinc-DE	[10]
32	1.2071×10^{-6}	2.9038×10^{-4}	8.5108×10^{-7}	9.7384×10^{-4}
64	5.5891×10^{-9}	7.2655×10^{-5}	7.0451×10^{-9}	2.4354×10^{-4}
128	7.5220×10^{-11}	1.8168×10^{-5}	6.2965×10^{-9}	6.0887×10^{-5}

TABLE XIII: The maximum absolute error at interpolation points for Example 4, with $L = 2\pi$, $\theta = \frac{1}{2}$ and $N = 1000$. Comparing with the previous table, we observed again that the Sinc-Hybrid method exhibits Runge's phenomenon, while the Sinc-DE method does not.

$m+1$	$T = 0.1$		$T = 0.5$	
	Sinc-DE	[10]	Sinc-DE	[10]
32	1.4826×10^{-6}	1.6586×10^{-2}	1.0843×10^{-6}	1.1056×10^{-2}
64	5.6114×10^{-9}	8.1809×10^{-3}	7.0934×10^{-9}	5.4760×10^{-3}
128	7.5496×10^{-11}	4.0627×10^{-3}	6.3182×10^{-9}	2.7223×10^{-3}

TABLE XIV: Maximum error $E_\infty(T)$ at collocation points for Example 4, with $T = 0.1$, $L = 2\pi$, and $\theta = \frac{1}{2}$ in the Coupled Burgers Equation using SCM-DE. From these data we again observe 2nd order convergence in Δt and higher order convergence in the number of spacial intervals, $m + 1$.

Δt	$m+1 = 10$	$m+1 = 20$	$m+1 = 40$	$m+1 = 80$	$m+1 = 160$
10^{-1}	3.133×10^{-2}	2.543×10^{-4}	7.538×10^{-5}	7.549×10^{-5}	7.551×10^{-5}
10^{-2}	6.723×10^{-3}	7.745×10^{-5}	7.532×10^{-7}	7.538×10^{-7}	7.540×10^{-7}
10^{-3}	1.482×10^{-2}	1.035×10^{-4}	2.985×10^{-7}	7.539×10^{-9}	7.540×10^{-9}
10^{-4}	1.482×10^{-2}	1.149×10^{-4}	2.934×10^{-7}	5.955×10^{-10}	7.536×10^{-11}
10^{-5}	1.482×10^{-2}	1.205×10^{-4}	2.949×10^{-7}	5.955×10^{-10}	1.929×10^{-12}

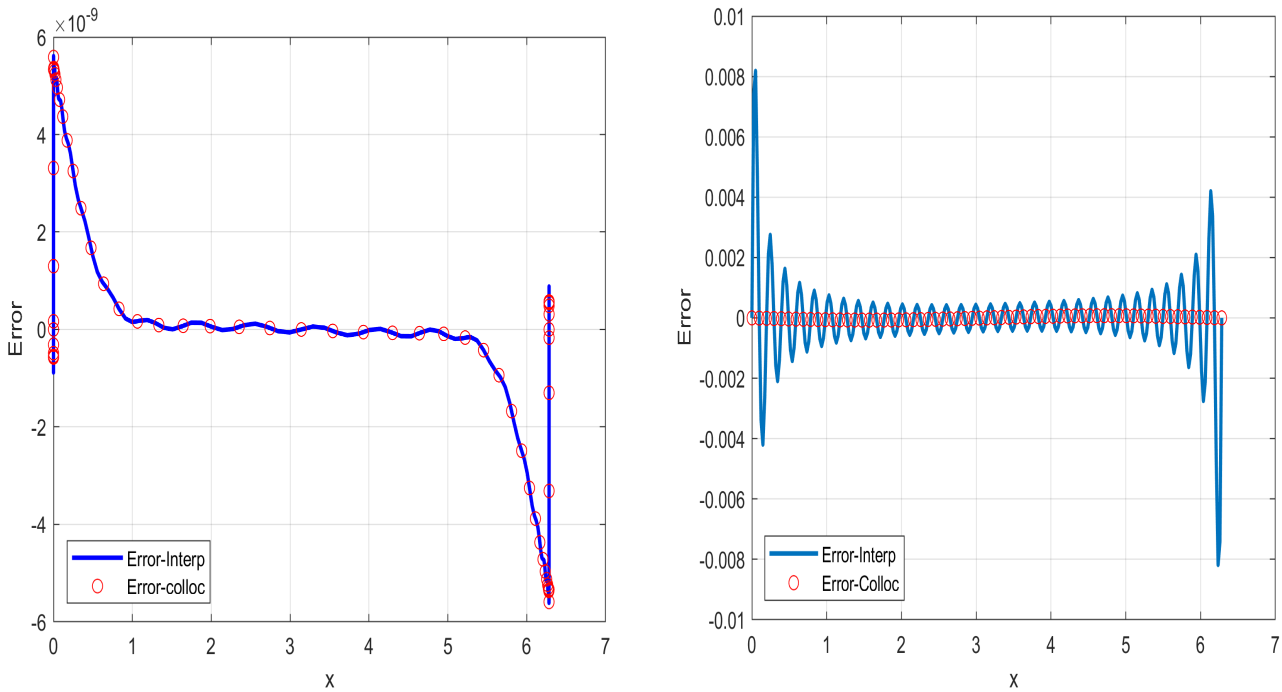

(a) SCM-DE error comparison

(b) Hybrid error comparison

Fig. 10: Errors for SCM-DE and Hybrid methods at collocation and interpolation points for Example 4. These figures illustrate the accuracy of each method with parameters $T = 0.1$, $m + 1 = 64$, $L = 2\pi$, $N = 1000$, and $\theta = \frac{1}{2}$. Again, the Sinc-Hybrid approximation exhibits Runge's phenomenon, which the Sinc-DE method does not.

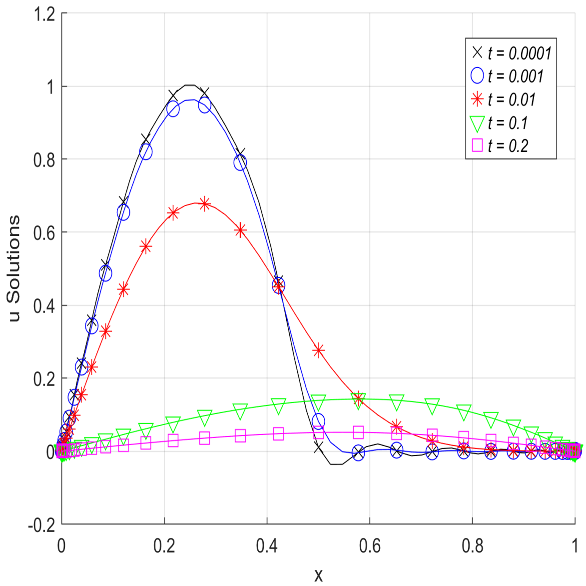

(a) Numerical solution $u(x,t)$

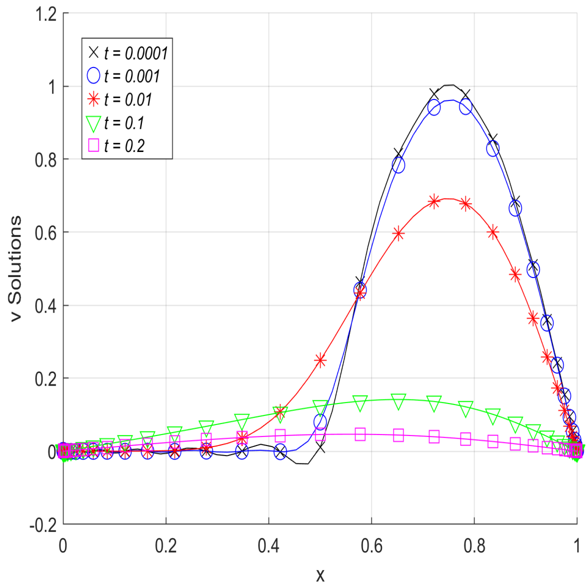

(b) Numerical solution $v(x,t)$

Fig. 11: Evolution of computed solutions for Example 4, where markers represent collocation points and curves represent the Sinc interpolation. The data is based on [34] in the vicinity of $t=0$. The parameters are set as $L=1$, $m+1=50$, $\theta=\frac{1}{2}$, $\Delta t=10^{-5}$, $D_1=D_2=1$, $\eta=\xi=2$, and $\alpha=\beta=10$. The example considers non-smooth initial conditions. We observed that the sinc solution oscillates in x for t close to 0.

TABLE XV: The approximate maximum values of u and v at different time levels for Example 4, with data from [34]. That is, with $L=1$, $m+1=50$, $\theta=\frac{1}{2}$ and $\Delta t=10^{-5}$, $D_1=D_2=1$, $\eta=\xi=2$, and $\alpha=\beta=10$, and a non-smooth initial conditions.

t	$u(x,t)$					$v(x,t)$				
	Sinc-DE	[34]	[35]	[11]	At point	Sinc-DE	[34]	[35]	[11]	At point
0.1	0.14309	0.144501	0.14449	0.14456	0.58	0.14172	0.143155	0.14314	0.14306	0.66
0.2	0.05192	0.052352	0.05235	0.05237	0.54	0.04660	0.047004	0.04700	0.04697	0.56
0.3	0.01917	0.019316	0.01931	0.01932	0.52	0.01712	0.017259	0.01726	0.01725	0.52
0.4	0.00713	0.007183	0.00718	0.00718	0.50	0.00637	0.006415	0.00641	0.00641	0.50

TABLE XVI: Maximum absolute error for $u(x,t)$ in Example 4 at different values of T and $m+1$. That is, with $L=1$, $m+1=50$, $\theta=\frac{1}{2}$ and $\Delta t=10^{-5}$, $D_1=D_2=1$, $\eta=\xi=2$, and $\alpha=\beta=10$, and a non-symmetric, non-smooth initial condition. An exact solution is not available, so the errors are measured in relation to the numerical solution for $m+1=160$.

$u(x,t)$						
T	N	$m+1=10$	$m+1=20$	$m+1=40$	$m+1=80$	Max $u(x,t)$
0.2	2×10^4	9.923×10^{-3}	2.102×10^{-3}	4.266×10^{-3}	9.737×10^{-4}	5.237×10^{-2}
0.1	1×10^4	3.387×10^{-2}	7.541×10^{-3}	4.343×10^{-3}	9.775×10^{-4}	1.444×10^{-1}
0.01	1×10^3	1.450×10^{-1}	5.040×10^{-2}	1.219×10^{-2}	2.869×10^{-3}	6.810×10^{-1}
0.001	1×10^2	1.998×10^{-1}	8.552×10^{-2}	3.530×10^{-2}	9.785×10^{-3}	9.613×10^{-1}
0.0001	1×10	2.264×10^{-1}	9.580×10^{-2}	5.315×10^{-2}	1.918×10^{-2}	9.961×10^{-1}

TABLE XVII: Maximum absolute error for $v(x,t)$ in Example 4 at different values of T and N_x. That is, with $L=1$, $m+1=50$, $\theta=\frac{1}{2}$ and $\Delta t=10^{-5}$, $D_1=D_2=1$, $\eta=\xi=2$, and $\alpha=\beta=10$, and a non-symmetric, non-smooth initial condition. An exact solution is not available, so the errors are measured in relation to the numerical solution for $m+1=160$.

$v(x,t)$						
T	N	$m+1=10$	$m+1=20$	$m+1=40$	$m+1=80$	Max $v(x,t)$
0.2	2×10^4	8.361×10^{-3}	1.943×10^{-3}	4.266×10^{-3}	9.737×10^{-4}	4.699×10^{-2}
0.1	1×10^4	3.387×10^{-2}	7.178×10^{-3}	4.343×10^{-3}	9.775×10^{-4}	1.432×10^{-1}
0.01	1×10^3	1.826×10^{-1}	4.888×10^{-2}	1.170×10^{-2}	2.749×10^{-3}	6.954×10^{-1}
0.001	1×10^2	2.242×10^{-1}	8.503×10^{-2}	3.493×10^{-2}	9.716×10^{-3}	9.612×10^{-1}
0.0001	1×10	2.292×10^{-1}	9.623×10^{-2}	5.310×10^{-2}	1.915×10^{-2}	9.961×10^{-1}

VIII. Conclusions

This work investigated a new Sinc Collocation Method (SCM) with Double Exponential (DE) transformations and compared it with the Sinc-Hybrid method for solving partial differential equations, focusing on Burgers' equation. In theory, sinc collocation methods achieve exponential convergence on smooth problems. Other works have demonstrated high-order convergence of sinc collocation for integral equations [36] and boundary value problems [37]. The SCM-DE method demonstrated high-order spatial accuracy (up to order 8) and second-order time convergence on an evolution equation. It proved to be robust and accurate at both collocation and interpolation points.

Comparisons with the method in [10] highlighted SCM-DE's superior accuracy across various initial conditions and discretization schemes, closely matching the exact solution. While the Sinc-Hybrid method [10] achieved reliable results at collocation points, it exhibited discrepancies due to oscillations at interpolation points, indicating Runge's phenomenon. In contrast, the SCM-DE method showed consistent performance across all tested scenarios.

The SCM-DE method also demonstrated more accurate results than the Milne method [16] and the standard Crank–Nicolson Finite Difference method. We showed that for a non-smooth problem (Example 4) as studied in [34], [35],[11], performance of SCM-DE is degraded, as is expected from the theory.

Future work could extend SCM-DE to problems with non-homogeneous Dirichlet boundary conditions and focus on optimizing computational efficiency.

References

[1] P. Klankaew and N. Pochai, "A Numerical Groundwater Quality Assessment Model Using the Cubic Spline Method," *IAENG International Journal of Applied Mathematics*, vol. 54, no. 1, pp. 111–116, 2024.

[2] G. B. Whitham, *Linear and Nonlinear Waves*, Pure and Applied Mathematics, Wiley-Interscience, New York, 1974, p. 431.

[3] E. R. Benton and G. W. Platzman, "A Table of Solutions of the One-Dimensional Burgers' Equation," *Quarterly of Applied Mathematics*, vol. 30, no. 2, pp. 195–212, 1972.

[4] E. Hopf, "The Partial Differential Equation $u_t + uu_x = \mu u_{xx}$," *Communications on Pure and Applied Mathematics*, vol. 3, no. 3, pp. 201–230, 1950.

[5] M. F. Hamilton and D. T. Blackstock, *Nonlinear Acoustics*, Academic Press, San Diego, 1998.

[6] H. Bateman, "Some Recent Researches on the Motion of Fluids," *Monthly Weather Review*, vol. 43, no. 4, pp. 163–170, 1915.

[7] J. M. Burgers, "A Mathematical Model Illustrating the Theory of Turbulence," *Advances in Applied Mechanics*, vol. 1, pp. 171–199, 1948.

[8] S. E. Esipov, "Coupled Burgers Equations: A Model of Polydispersive Sedimentation," *Physical Review E*, vol. 52, no. 4, pp. 3711–3718, 1995.

[9] A. R. Adem, B. Muatjetjeja and T. S. Moretlo, "An Extended (2+1)-Dimensional Coupled Burgers System in Fluid Mechanics: Symmetry Reductions; Kudryashov Method; Conservation Laws," *International Journal of Theoretical Physics*, vol. 62, article number 38, 2023.

[10] L. Wang, H. Li and Y. Meng, "Numerical Solution of Coupled Burgers' Equation Using Finite Difference and Sinc Collocation Method," *Engineering Letters*, vol. 29, no. 2, pp. 668–674, 2021.

[11] R. C. Mittal and G. Arora, "Numerical Solution of the Coupled Viscous Burgers' Equation," *Communications in Nonlinear Science and Numerical Simulation*, vol. 16, no. 3, pp. 1304–1313, 2011.

[12] V. K. Srivastava, M. K. Awasthi and M. Tamsir, "A Fully Implicit Finite-Difference Solution to One-Dimensional Coupled Nonlinear Burgers' Equations," *International Journal of Mathematical, Computational Science and Engineering*, vol. 7, no. 4, pp. 283–287, 2013.

[13] D. Deng and T. Pan, "A Fourth-order Singly Diagonally Implicit Runge-Kutta Method for Solving One-dimensional Burgers' Equation," *IAENG International Journal of Applied Mathematics*, vol. 45, no. 4, pp. 327–333, 2015.

[14] Ö. Oruç, F. Bulut and A. Esen, "Chebyshev Wavelet Method for Numerical Solutions of Coupled Burgers' Equation," *Hacettepe Journal of Mathematics & Statistics*, vol. 48, no. 1, pp. 1–16, 2019.

[15] A. J. Hussein and H. A. Kashkool, "Weak Galerkin Finite Element Method for Solving One-Dimensional Coupled Burgers' Equations," *Journal of Applied Mathematics and Computing*, vol. 63, pp. 265–293, 2020.

[16] S. Chonladed and K. Wuttanachamsri, "A Numerical Solution of Burger's Equation Based on Milne Method," *IAENG International Journal of Applied Mathematics*, vol. 51, no. 2, pp. 411–415, 2021.

[17] J. Crank and P. Nicolson, "A Practical Method for Numerical Evaluation of Solutions of Partial Differential Equations of the Heat-Conduction Type," *Mathematical Proceedings of the Cambridge Philosophical Society*, vol. 43, no. 1, pp. 50–67, 1947.

[18] G. D. Smith, *Numerical Solution of Partial Differential Equations: Finite Difference Methods*, Oxford University Press, Oxford, 1985.

[19] A. R. Mitchell and D. F. Griffiths, *The Finite Difference Method in Partial Differential Equations*, Wiley, Chichester, 1980.

[20] J. P. Boyd, *Chebyshev and Fourier Spectral Methods*, 2nd ed., Dover Publications, Mineola, NY, 2001.

[21] F. Stenger, *Numerical Methods Based on Sinc and Analytic Functions*, Springer Series in Computational Mathematics, vol. 20, Springer-Verlag, New York, 1993.

[22] J. Lund and K. L. Bowers, *Sinc Methods for Quadrature and Differential Equations*, Society for Industrial and Applied Mathematics, Philadelphia, 1992.

[23] H. Takahasi and M. Mori, "Double Exponential Formulas for Numerical Integration," *Publications of the Research Institute for Mathematical Sciences*, vol. 9, no. 3, pp. 721–741, 1973.

[24] M. Mori and M. Sugihara, "The Double-Exponential Transformation in Numerical Analysis," *Journal of Computational and Applied Mathematics*, vol. 127, no. 1–2, pp. 287–296, 2001.

[25] E. T. Whittaker, "On the Functions Which Are Represented by the Expansions of the Interpolation-Theory," *Proceedings of the Royal Society of Edinburgh*, vol. 35, pp. 181–194, 1915.

[26] F. Stenger, "Summary of Sinc Numerical Methods," *Journal of Computational and Applied Mathematics*, vol. 121, no. 1–2, pp. 379–420, 2000.

[27] S. Kang, K. Abdella, M. Pollanen, S. Zhang, and L. Wang, "Sinc Collocation Numerical Methods for Solving Two-Dimensional Gross-Pitaevskii Equations with Non-Homogeneous Dirichlet Boundary Conditions," *Advances in Applied Mathematics and Mechanics*, vol. 14, no. 6, pp. 1302–1332, 2022.

[28] M. Sugihara, "Double Exponential Transformation in the Sinc-Collocation Method for Two-Point Boundary Value Problems," *Journal of Computational and Applied Mathematics*, vol. 149, no. 1–2, pp. 239–250, 2002.

[29] S. Boscarino, F. Filbet, and G. Russo, "High Order Semi-implicit Schemes for Time Dependent Partial Differential Equations," *Journal of Scientific Computing*, vol. 68, no. 3, pp. 975–1001, 2016.

[30] A. Iserles, *A First Course in the Numerical Analysis of Differential Equations*, 2nd ed., Cambridge Texts in Applied Mathematics, vol. 44, Cambridge University Press, Cambridge, 2008.

[31] C. Li and X. Wu, "Numerical Solution of Differential Equations Using Sinc Method Based on the Interpolation of the Highest Derivatives," *Applied Mathematical Modelling*, vol. 31, no. 1, pp. 1–9, 2007.

[32] M. Sugihara, "Optimality of the Double Exponential Formula – Functional Analysis Approach," *Numerische Mathematik*, vol. 75, no. 3, pp. 379–395, 1997.

[33] I. A. Hassanien, A. A. Salama, and H. A. Hosham, "Fourth-order finite difference method for solving Burgers' equation," *Applied Mathematics and Computation*, vol. 170, no. 2, pp. 781–800, 2005.

[34] O. E. Hepson and I. Dağ, "An Exponential Cubic B-spline Algorithm for Solving the Nonlinear Coupled Burgers' Equation," *Computational Methods for Differential Equations*, vol. 9, no. 4, pp. 1109–1127, 2021.

[35] R. C. Mittal and A. Tripathi, "A Collocation Method for Numerical Solutions of Coupled Burgers' Equations," *International Journal for Computational Methods in Engineering Science and Mechanics*, vol. 15, no. 5, pp. 457–471, 2014.

[36] T. Okayama, "Sinc-collocation methods with consistent collocation points for Fredholm integral equations of the second kind," *Dolomites Research Notes on Approximation*, vol. 16, no. 3, pp. 63–74, 2023.

[37] M. Nabati and A. Barati, "A sinc-collocation approximation solution for strongly nonlinear class of weakly singular two-point boundary value problems," *Filomat*, vol. 37, no. 29, pp. 10077–10092, 2023.